Journal of Computational Physics **182,** 586–621 (2002)
doi:10.1006/jcph.2002.7186

On the Development of Spray Submodels Based on Droplet Size Moments

J. C. Beck and A. P. Watkins

Atomisation and Sprays Research Group, Mechanical, Aerospace and Manufacturing Engineering Department, UMIST, Manchester, United Kingdom
E-mail: paul.watkins@umist.ac.uk

Received September 19, 2001; revised May 31, 2002

Hitherto, all polydisperse spray models have been based on discretising the liquid flow field into groups of equally sized droplets. The authors have recently developed a spray model that captures the full polydisperse nature of the spray flow without using droplet size classes (Beck, 2000, Ph.D thesis, UMIST; Beck and Watkins, 2001, *Proc. R. Soc. London A*). The parameters used to describe the distribution of droplet sizes are the moments of the droplet size distribution function. Transport equations are written for the two moments which represent the liquid mass and surface area, and two more moments representing the sum of drop radii and droplet number are approximated via use of a presumed distribution function, which is allowed to vary in space and time. The velocities to be used in the two transport equations are obtained by defining moment-average quantities and constructing further transport equations for the relevant moment-average velocities. An equation for the energy of the liquid phase and standard gas phase equations, including a k–ε turbulence model, are also solved. All the equations are solved in an Eulerian framework using the finite-volume approach, and the phases are coupled through source terms. Effects such as interphase drag, droplet breakup, and droplet–droplet collisions are also captured through the use of source terms. The development of the submodels to describe these effects is the subject of this paper. All the source terms for the hydrodynamics of the spray are derived in this paper in terms of the four moments of the droplet size distribution in order to find the net effect on the whole spray flow field. The development of similar submodels to describe heat and mass transfer effects between the phases is the subject of a further paper (Beck and Watkins, 2001, *J. Heat Fluid Flow*). The model has been applied to a wide variety of different sprays, including high-pressure diesel sprays, wide-angle solid-cone water sprays, hollow-cone sprays, and evaporating sprays. The comparisons of the results with experimental data show that the model performs well. The interphase drag model, along with the model for the turbulent dispersion of the liquid, produces excellent agreement in the spray penetration

0021-9991/02 $35.00

results, and the moment-average velocity approach gives good radial distributions of droplet size, showing the capability of the model to predict polydisperse behaviour. Good submodel performance results in droplet breakup, collisions, and evaporation effects (see (Beck and Watkins, 2001, *J. Heat Fluid Flow*)) also being captured successfully.

Key Words: sprays; modelling; submodels; droplet size moments.

1. INTRODUCTION

Many computational spray models employ the discrete droplet model (DDM) pioneered by Dukowicz [4]. This involves solving the equations of motion for a turbulent carrier gas in an Eulerian scheme, and integrating Lagrangian equations of motion for liquid droplets along true path lines. These two calculation schemes, and therefore the two phases, are then coupled through source terms in the gas phase transport equations (Crowe *et al.* [5]). The major advantages of this over a purely Eulerian scheme are the ability to efficiently discretise the liquid phase into groups of identical droplets, each containing droplets of a given radius, and the fact that the equations for the dispersed liquid phase are more naturally written down in a Lagrangian manner. The disadvantages of the discrete droplet model is that it is dependent on predicting the chaotic motions of individual droplets to provide an overall picture of the spray (see Gosman and Ioannides [6]). The stochastic models employed in producing this chaotic motion are computationally expensive.

Multisize Eulerian treatments have also been employed by similar discretisation of the droplet size distribution and considering each size group as a completely separate phase (Mostafa and Mongia [7]). However, this leads to a scheme involving many phases and is thus also computationally expensive.

The stochastic nature of the sprays has led some researchers to search for a probabilistic formulation to the problem. This forms the basis of the third method. It is based on the spray equation of Williams [8]. This involves defining

$$f_j(r, \mathbf{x}, \mathbf{v}, t)\, dr\, d\mathbf{x}\, d\mathbf{v}, \tag{1}$$

where f_j is the probable number of droplets in the diameter range dr about r, with velocity $d\mathbf{v}$ about $\mathbf{v}$ in position $d\mathbf{x}$ about $\mathbf{x}$. Changes in the function are due to convection of *j-particles* into the considered volume, acceleration/deceleration of particles into the velocity range, and growth/shrinking of particles into the diameter range. An Eulerian conservation equation is then written for f_j in each considered range j, by integrating over a narrow radius range rather than by taking a delta function approach. Lagrangian equations are written to evaluate the velocity and the rates of change of velocity, radius, and energy. Source terms are included to model the effects of droplet breakup and the effects on the gas phase. An early attempt to employ this approach is summarised in Gupta and Bracco [9]. They were able to obtain closed-form solutions of equations for parcels of drops and then integrate (or summate) over the total number of parcels to obtain the full solution. However, they were able to do this only for dilute sprays and by ignoring the important spray phenomena of drop breakup and collisions.

An alternative approach to the modelling of polydisperse sprays that also takes the probabilistic approach to the spray equation, but which is able to incorporate thick spray effects and drop breakup and collisions, has been suggested by Beck [1] and Beck and Watkins [2]. Both the liquid and the gas are represented in the Eulerian formulation, and the full polydisperse nature of the spray flow is captured whilst only considering the liquid as one phase. This requires some representation of the droplet size distribution. The first four moments of the droplet size number distribution are found to provide an adequate representation of the polydisperse nature of the spray, and by solving equations for these parameters, a fully multisize model of the spray has been constructed. There are a number of advantages of modelling the spray in this fashion. First, the number of equations being solved is significantly fewer than any of the previous polydisperse spray models, making the scheme more computationally efficient than its predecessors. Second, the use of these moments means that the spray is dealt with in terms of average quantities, allowing a smooth representation of the droplet size distribution at all points, rather than a discrete representation. These distribution function moments are very useful parameters in characterising the spray as they are inherently related to the spray mean diameters. They are also the terms needed to produce the source terms for the effect of the spray on the gas phase when considering the spray as a whole.

The original intention of the model was to obtain all of the first four moments by means of transport equations. Had that been possible there would have been no need to specify a number distribution, since only the moments are required. To date, however, it has not been possible to obtain all four moments by means of transport equations. Instead, as explained in Section 3.2, only two moments are obtained in this way. This means that a number distribution has to be assumed to get the other two moments. This is clearly a drawback of the model. Nevertheless, the form of the distribution is allowed to change in space and time as the spray progresses and it can be truncated in different ways to match the values of the calculated moments. Different forms of the initial distribution can also be chosen to represent different spray types.

In [2] only the main model was presented, and no details were given of the forms taken by the submodels to describe important spray phenomena. These phenomena include the interphase drag, droplet breakup and collisions, and heat and mass transfer between the phases. The role of this paper is to complete the description of the hydrodynamics of the spray modelling by describing how the required models are expressed in terms of the moments of the number distribution. The heat and mass transfer mechanisms are similarly treated in [3]. Applications of the model to wide-angle full-cone sprays and evaporating sprays are reported in [10].

The main model, as derived in [2], is outlined in the next section. Section 3 deals with the derivation of the spray submodels for interphase drag, drop breakup, and drop collisions. Included here is material on the initial and boundary conditions imposed on the spray model, with particular emphasis on the values assigned to the moments of the number distribution and the moment-averaged velocities. In addition, the treatment of the approximate number distribution chosen for the model is outlined. Section 4 discusses the computational method used to solve the govering conservation equations for both phases. Section 5 deals with the test cases examined. These include narrow-cone diesel spray cases and hollow-cone fuel spray cases. In both sets of cases the ability of the model to predict experimental data is examined. Included here also are examinations of the effects of the spray submodels and the effects of time step and grid densities on the predictions.

2. MODEL FORMULATION

2.1. *Droplet Size Distribution Function Moments*

Define $n(r)$ as a multiple of the probability density function of droplet radius, such that the integral over all droplets provides the total number of droplets per unit total volume (*not* unit liquid volume). This is designated by Q_0, following the notation of Adam and Schnerr [11], such that

$$\int_0^\infty n(r)\,dr = Q_0. \tag{2}$$

This is the first of the distribution function moments. The ith moment can be written similarly, as

$$Q_i = \int_0^\infty n(r) r^i\,dr. \tag{3}$$

It is worth noting a few properties of the quantities defined here. For any representation of a droplet size distribution function the assumption is made that the droplets are approximately spherical. Using this assumption, it can be seen that the moments Q_2 and Q_3 represent physical quantities, the knowledge of which is very useful for modelling sprays. The surface area of the droplets per unit total volume is $4\pi Q_2$, and the liquid volume per unit total volume (that is, the fractional volume of liquid) is given as

$$\frac{V_l}{V_{cell}} = \frac{4\pi Q_3}{3}. \tag{4}$$

As mean droplet diameters are often used to characterise the droplet sizes in a spray, it is useful to note that the four parameters (Q_0 to Q_3) provide all mean droplet diameters from D_{10} to D_{32}, as, by definition,

$$D_{pq}^{p-q} = \frac{2^{p-q} Q_p}{Q_q}. \tag{5}$$

A good discussion of droplet distribution moments and their relationship to mean droplet diameters in sprays is given by Sowa [12]. Hence it can be seen that the first four moments contain a great deal of information about the spray. Starting from this point, [1] and [2] use these parameters to build a fully polydisperse spray model without the need to separate the droplets into size classes.

In many respects the most important of the first four moments is Q_3, because assuming all droplets have the same density (locally), this parameter defines the mass of liquid present per unit volume. This means that the transport equation for Q_3, presented in the following section, is in fact equivalent to a liquid phase continuity equation. This suggests strongly that any modelling done using these moments must at least consider this fourth moment, and it will be seen later that the modelling of the spray phenomena will also require values for the first three.

2.2. *Moment-Average Quantities*

To write Eulerian transport equations for the droplet moments, the speed at which the moments are to be convected must be defined. This is not a trivial problem as, in general, the droplets are travelling at a variety of different velocities. Logically the net convection of mass would occur at the mass-average velocity, and the net convection of droplet surface area (say) would occur at the surface-area-average velocity, and there is no reason for these two values to be the same. Larger droplets experience less drag and generally have higher velocities than the smaller droplets, and this is reflected by the mass-average velocity being higher than the surface-area-average velocity. From the definitions of the droplet moments, the mass-average velocity is the correct velocity at which to convect Q_3 and the surface-area-average velocity is the correct velocity at which to convect Q_2. The same idea can also be applied to moment-average energies to capture the effect of small droplets heating up more quickly than large droplets. Hence these moment-average quantities convect the moments such that they are not all convected at the same rate. This results in the moments providing a representation of the distribution of droplet sizes at each point, and the moment-average velocities providing the means by which the distribution of droplet sizes can change in time and space. The two concepts allied together are capable of providing a picture of the behaviour of a polydisperse spray.

The moment average, Φ_i, of a quantity Φ averaged over the ith moment Q_i is defined as

$$\Phi_i = \frac{\int_0^\infty r^i n(r) \Phi \, dr}{Q_i}. \tag{6}$$

This model is not concerned with knowing the velocity of every droplet, as is usually the case in the discrete droplet model where velocities are required for each of the representative drops that are tracked, but uses a selection of average velocities and their relationship to each other to determine how the size distribution evolves at each point in space. The key question is whether this continuum averaging gives as good a representation of the spray and its dynamics as can be obtained by discretising the droplets into size groups.

2.3. *Liquid-Phase Transport Equations*

To write equations for mass and momentum in a two-phase flow, it is necessary to define the void fraction θ, which is the volume fraction of gas in each computational grid cell (or indeed any control volume). This is given by

$$\theta = 1 - \frac{V_l}{V_{cell}}, \tag{7}$$

which can be calculated directly from the third moment of the droplet size distribution function through (4). The transport equation for the third droplet moment is written as the liquid mass conservation equation

$$\frac{\partial}{\partial t}(\rho_l(1-\theta)) + \frac{\partial}{\partial x_j}(\rho_l(1-\theta)U_{l3j}) = -S_m. \tag{8}$$

The convection velocity required is the moment-average value U_{l3}, obtained from (6) by

setting $i = 3$ and $\Phi = U_l$. The source term S_m in (8) has only one contribution due to evaporation as the other phenomena considered do not affect the total mass of liquid present.

The equations for the remaining moments take a similar form, but more care must be taken because of the requirement for more source terms due to the changes effected by droplet breakup, droplet–droplet collisions, and evaporation and changes in the droplet density. The source terms that are related to the hydrodynamics of the spray are discussed in detail in Section 3. Those related to heat and mass transfer between the phases are the subject of another publication [3] but are also discussed by Beck [1]. The equations are

$$\frac{\partial}{\partial t}(Q_i) + \frac{\partial}{\partial x_j}(Q_i U_{lij}) = -S_{Q_i}. \tag{9}$$

Use of the ith moment-average velocity in these equations should be noted. In the present version of the model, these equations are solved only for $i = 2$, i.e., for the surface-area moment, for reasons explained in Section 3.2. S_{Q_i} is a source term calculated from the submodels of Section 3.

The liquid-phase momentum equation, as used in the calculation scheme, is based on the work of Harlow and Amsden [13] for particulate flows. It is derived in [1] and [2] and is written as

$$\begin{aligned}\frac{\partial}{\partial t}(\rho_l(1-\theta)U_{l3i}) + \frac{\partial}{\partial x_j}(\rho_l(1-\theta)U_{l3i}U_{l3j}) + U_{l3i}S_m \\ = \frac{\partial}{\partial x_j}\left(\rho_l(1-\theta)\sigma_v \nu_l \frac{\partial U_{l3i}}{\partial x_j}\right) - S_{U_i}.\end{aligned} \tag{10}$$

The equations for the other moment-average velocities follow the same pattern, the subscript k denoting the moment number. Thus

$$\begin{aligned}\frac{\partial}{\partial t}(Q_k U_{lkj}) + \frac{\partial}{\partial x_j}(Q_k U_{lki}U_{lkj}) + \frac{\partial}{\partial x_j}(Q_k(U_{l3i}-U_{lki})(U_{l3j}-U_{lkj})) \\ + U_{l3i}B_{Q_k} + U_{lki}\left(S_{Q_k} - B_{Q_k}\right) \\ = \frac{\partial}{\partial x_j}\left(Q_k \sigma_v \nu_l \frac{\partial U_{lki}}{\partial x_j}\right) - S_{U_{ki}},\end{aligned} \tag{11}$$

but there are important differences, notably the third term on the left-hand side of (11). The reasons for the existence of this term are given in [1] and [2]. Again, this equation is solved only for $k = 2$ in the present version of the model.

In the complete model, an equation for liquid-phase energy conservation is also solved [1–3], but this will not be considered here.

2.4. *Gas-Phase Transport Equations*

The gaseous mass transport equation is written as

$$\frac{\partial}{\partial t}(\theta\rho_g) + \frac{\partial}{\partial x_j}(\theta\rho_g U_{gj}) = S_m, \tag{12}$$

where S_m is the mass transferred from the liquid phase to the gas phase per unit time within a control volume. The gaseous momentum equation, including turbulence effects, is written

as

$$\frac{\partial}{\partial t}(\theta\rho_g U_{gi}) + \frac{\partial}{\partial x_j}(\theta\rho_g U_{gj}U_{gi}) - U_{gi}\left(\frac{\partial}{\partial t}(\theta\rho_g) + \frac{\partial}{\partial x_j}(\theta\rho_g U_{gj})\right)$$
$$= \frac{\partial}{\partial x_j}\left(\mu_{eff}\theta\left(\frac{\partial U_{gi}}{\partial x_j} + \frac{\partial U_{gj}}{\partial x_i}\right)\right) - \theta\frac{\partial P}{\partial x_i} - \frac{\partial}{\partial x_j}\left(\frac{2}{3}\theta\rho_g k\delta_{ij}\right) + S_m(U_{li} - U_{gi}) + S_{U_i}. \tag{13}$$

The effective viscosity μ_{eff} is given by

$$\mu_{eff} = \mu_{lam} + \rho_g C_\mu \frac{k^2}{\varepsilon}, \tag{14}$$

where $C_\mu = 0.09$ and k and ε are the turbulent kinetic energy and its dissipation rate respectively.

The source term S_{U_i} in (13) is the momentum exchanged from the liquid to the gas per unit time in a control volume. In a single-phase flow, the third term on the left-hand side of (13) is zero as it is a multiple of the continuity equation. Due to interphase mass transfer this can be nonzero in two-phase flow and is hence included. The penultimate term on the right-hand side of (13) is described by Mostafa and Mongia [7] as the momentum growth term, and it results from the initial relative velocity between the generated vapour (initially travelling at liquid velocity) and the carrier gas.

In the complete model, equations are solved for the gas-phase energy conservation and also for the vapour mass fraction. Gaseous properties are also written as a function of vapour mass fraction [1–3].

The turbulence model employed is the two-equation model of Launder and Spalding [14], with the equations being solved for the turbulence kinetic energy and its dissipation rate. The equations are

$$\frac{\partial}{\partial t}(\theta\rho_g k) + \frac{\partial}{\partial x_j}(\theta\rho_g U_{gj}k) - kS_m = \frac{\partial}{\partial x_j}\left(\frac{\mu_{eff}}{\sigma_k}\theta\left(\frac{\partial k}{\partial x_j}\right)\right) + \theta P_k - \rho_g\varepsilon\theta \tag{15}$$

and

$$\frac{\partial}{\partial t}(\theta\rho_g\varepsilon) + \frac{\partial}{\partial x_j}(\theta\rho_g U_{gj}\varepsilon) - \varepsilon S_m$$
$$= \frac{\partial}{\partial x_j}\left(\frac{\mu_{eff}}{\sigma_\varepsilon}\theta\left(\frac{\partial \varepsilon}{\partial x_j}\right)\right) + \theta C_{\varepsilon 1}P_k\frac{\varepsilon}{k} - \theta C_{\varepsilon 2}\frac{\rho_g\varepsilon^2}{k} + \theta C_{\varepsilon 3}\rho_g\varepsilon\frac{\partial U_{gj}}{\partial x_j}. \tag{16}$$

The turbulence kinetic energy production rate is given by

$$P_k = \rho_g C_\mu \frac{k^2}{\varepsilon}\left(\frac{\partial U_{gi}}{\partial x_j} + \frac{\partial U_{gj}}{\partial x_i}\right)\frac{\partial U_{gj}}{\partial x_i}. \tag{17}$$

The constants take the values $C_{\varepsilon 1} = 1.44$, $C_{\varepsilon 2} = 1.92$, $C_{\varepsilon 3} = -0.373$, $\sigma_t = 0.9$, $\sigma_k = 1.0$, and $\sigma_\varepsilon = 1.3$. The term involving $C_{\varepsilon 3}$ is an addition due to the effect of the liquid phase on the gas-phase turbulence. All the source terms are calculated by considering the effect of the gas phase on the liquid phase in terms of the droplet size distribution function moments. This is discussed in detail, and the source terms are derived, in Section 3.

3. SPRAY SUBMODELS

To form a complete simulation of spray behaviour, many phenomena found in sprays require modelling. In general, these models are more naturally described in a Lagrangian framework, and hence the majority are written in this form, although all are incorporated into an Eulerian frame within the current model.

3.1. *Initial and Boundary Conditions*

Although not strictly a submodel, a brief discussion of the inlet conditions will be given here, as the model assumes the spray to be fully atomised at the nozzle exit. The treatment of the spray injection is based on the injection cell treatment of Watkins [15]. The injector is located within this cell, it is assumed that the gas has entrained to the liquid velocity by the downstream face of the cell, and the velocities and void fraction are calculated there by one-dimensional inviscid flow analysis.

The main difference in this work from the injection cell treatment of [15] is that the injection domain is composed of more than one cell. The main reason is that this allows a greater range of radial velocities to be applied to the spray at inlet, given that the liquid velocities are applied at cell faces, and that there are no droplet groups. The fineness of grid with which this model is able to work allows the injection domain to be composed of a number of cells (up to five radial cells have been used successfully) and yet be smaller than the injection domain used in most DDM calculations. A schematic of the injection domain for a full-cone spray is presented as Fig. 1.

The injection velocity of the liquid is calculated via a Bernoulli argument, such that

$$U_{inj} = C_D \sqrt{\frac{2(P_{inj} - P_g)}{\rho_l}}, \tag{18}$$

where the coefficient of discharge is taken as 0.7 if not quoted in the literature. Similarly,

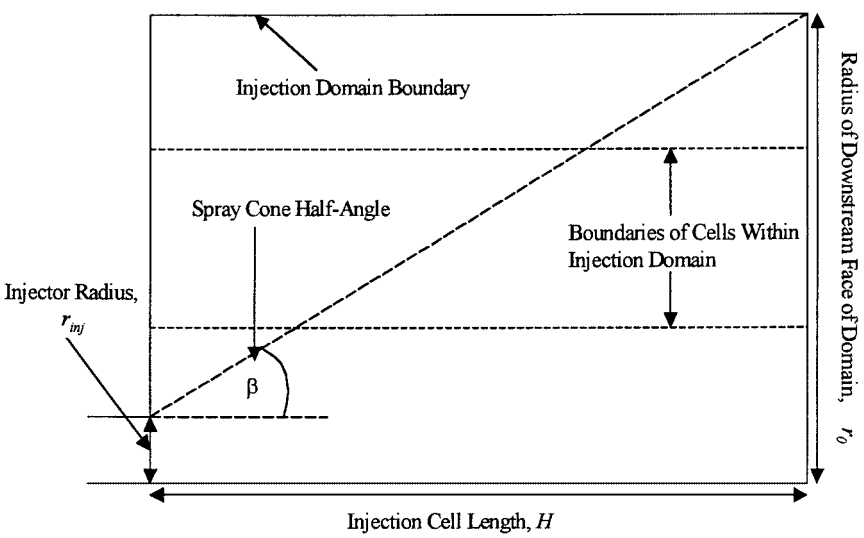

FIG. 1. Injection domain and parameters for a solid cone spray.

the spray cone half-angle, β, is usually taken from the literature, but for pressure-atomised sprays the correlation of Ranz [16] is used if the angle is unspecified.

The conditions at the downstream face of the domain are obtained from two equations that can be found in O'Rourke [17], the first from the continuity of liquid mass,

$$\rho_l U_{inj} \pi r_{inj}^2 = \rho_l (1-\theta) \pi r_0^2 U_0, \tag{19}$$

and the second from the conservation of axial momentum,

$$\rho_l U_{inj}^2 \pi r_{inj}^2 = \rho_l (1-\theta) \pi r_0^2 U_0^2 + \rho_g \theta \pi r_0^2 U_0^2. \tag{20}$$

where r_0 is the radius of the downstream face given by

$$r_0 = r_{inj} + H \tan \beta \tag{21}$$

and H is the axial length of the injection cell specified in the initial conditions. These equations can be solved simultaneously to give the downstream axial velocity and the void fraction at the downstream face as

$$U_0 = U_{inj} \left(\frac{-\left[1 - \frac{\rho_g}{\rho_l}\right] + \left\{ \left[1 - \frac{\rho_g}{\rho_l}\right]^2 + \frac{4\rho_g r_0^2}{\rho_l r_{inj}^2} \right\}^{\frac{1}{2}}}{\frac{2\rho_g r_0^2}{\rho_l r_{inj}^2}} \right) \tag{22}$$

and

$$\theta = 1 - \frac{U_{inj}}{U_0} \left(\frac{r_{inj}^2}{r_0^2} \right), \tag{23}$$

respectively. The radial velocities are given as

$$V_{0i} = U_0 \tan \left(\beta \frac{r_i}{r_0} \right), \tag{24}$$

where r_i is the radial distance from the axis of the ith radial grid line in the injection domain. The velocity of the gas entrained into the injection cell from the sides is calculated via a continuity argument as

$$V_{g0} = -\frac{r_0}{2H} U_0. \tag{25}$$

The injection conditions for a hollow cone spray are set up in a similar fashion. It should be noted that no attempt is made here to simulate the breakup of liquid sheets, as is done, for example, by Senecal *et al.* [18]. Rather, the sheet is presumed to break up across the injection domain and to be fully atomised at the downstream face.

The injection cell layout for a hollow-cone spray is shown in Fig. 2. As the sheet is usually thin, the domain is set up such that only one cell has liquid crossing its downstream face. The injection velocities and sheet thickness at nozzle exit are taken from the literature. Equations

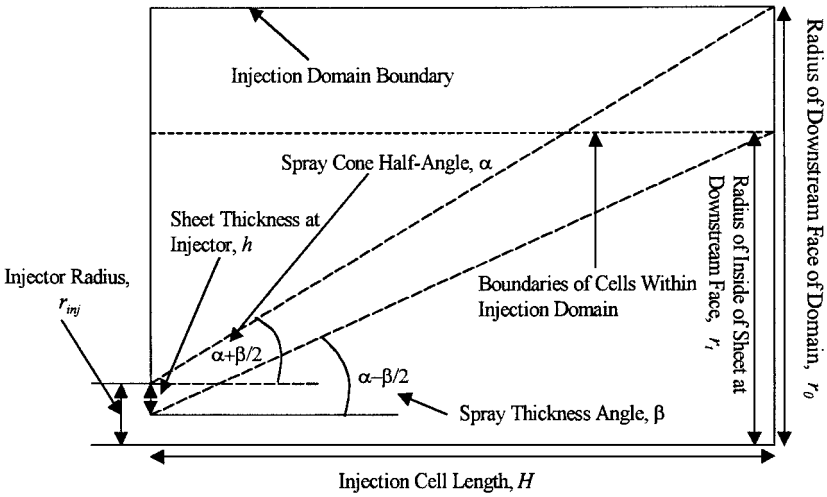

FIG. 2. Injection domain and parameters for a hollow cone spray.

similar to (22) and (23) can be written for the hollow-cone case, and the downstream face velocity and void fraction are given by

$$U_0 = U_{inj}\left(\frac{-\left[1-\frac{\rho_g}{\rho_l}\right]+\left\{\left[1-\frac{\rho_g}{\rho_l}\right]^2+\frac{4\rho_g\left(r_0^2-r_t^2\right)}{\rho_l\left(2r_{inj}h-h^2\right)}\right\}^{\frac{1}{2}}}{\frac{2\rho_g\left(r_0^2-r_t^2\right)}{\rho_l\left(2r_{inj}h-h^2\right)}}\right) \tag{26}$$

and

$$\theta = 1-\frac{U_{inj}}{U_0}\left(\frac{2r_{inj}h-h^2}{r_0^2-r_t^2}\right), \tag{27}$$

where r_t and r_0 are given by

$$r_t = (r_{inj}-h)+H\tan\left(\alpha-\frac{\beta}{2}\right) \tag{28}$$

and

$$r_0 = r_{inj}+H\tan\left(\alpha+\frac{\beta}{2}\right) \tag{29}$$

and h is the liquid sheet thickness at the nozzle. The radial velocity is given as

$$V_0 = U_0\tan\alpha, \tag{30}$$

and the velocities of the gas entering the domain from the sides are given by

$$V_{g0} = -\frac{\left(r_0^2-r_t^2\right)}{2Hr_0}U_0. \tag{31}$$

Using the calculated value of the void fraction at the downstream face of the injection domain, the value of Q_3 can be calculated via (4). The value of Q_2 is then calculated via

a prescribed inlet Sauter mean radius (SMR), usually the reference SMR, and the initial conditions for the other two moments can then be calculated from the truncated assumed distribution (see Section 3.2). The inlet values of the mass- and surface area-averaged axial and radial velocity components are set equal to U_0 and V_0, respectively.

Boundary conditions are required at the edges of the spray where no flux of liquid momentum or energy is allowed from a control volume in which no liquid is present. This is required due to the staggered grid employed. The other boundary conditions imposed on the liquid phase are the centre-line symmetry condition and zero normal gradients at outlet.

3.2. *Droplet Size Distribution Assumptions*

Accurate representation of the spectrum of droplet sizes is essential in the modelling of polydisperse sprays. Initially the calculation scheme was intended to provide enough information about the droplet size distribution to model the spray by predicting the first four moments of the number distribution function via transport equations. The breakup and collisions models detailed here require some way of predicting the surface area or total radius of part of the distribution, and not the whole. The only way to do this is to produce some function that approximates the droplet size distribution function and has moments that match those provided by the distribution function. Therefore the function has four constraints, one of which is a normalisation constraint. Finding a function that satisfies these constraints is a nontrivial problem and has not been solved successfully.

The fact that the model would allow the four moments to be transported at different velocities means that the polydisperse nature of the flow can be simulated. This, however, causes its own problems. At the edge of the spray, where the droplet population is small, significant differences in the moment-average velocities can result in a control volume that previously contained no liquid receiving a significant liquid mass but having a very small droplet number. The droplet sizes inferred from this by the submodels can become unrealistically large and the source terms produced then become very large, resulting in the scheme failing. It has proved too great a task to date to ensure that all four velocities are similar enough at the spray edges for the scheme to be reliable in most cases. The approximations made in the derivation of (11) are certainly more valid for the surface area and volume moments (Q_2 and Q_3) than for the other two. This suggests the idea that transport equations can be solved for just these two moments and their respective moment-average velocities by using an approximate distribution function based on the calculated moments to be used to estimate the remaining moments. This has two advantages over the four-moment approach. First, the moment-average velocities used are both fewer and more reliable, allowing a greater likelihood of being able to keep the scheme stable at the spray periphery. Second, fewer transport equations are being solved, which reduces the amount of computational work done.

The SMR is generally considered the most important parameter in the size distribution function, and so it would seem sensible to use the SMR as the parameter required in a two-moment distribution function. Other desirable qualities in this distribution function are accurate representation of typical droplet size distributions and ease of analytic integration, thereby avoiding having to perform numerical integrations.

An analytically integrable function to use as a number distribution was sought such that the volume distribution it produced was a reasonable approximation to a Rosin–Rammler distribution. This is a regularly used distribution in spray models, and as such it is a sensible

choice. It should be noted that any analytically integrable probability density function may be used in the scheme, so there is scope for research into using different reference distributions for different types of spray flow. The Rosin–Rammler volume distribution is defined as

$$v(r) = \left(\frac{\alpha_R}{r_R^{\alpha_R}}\right) r^{\alpha_R - 1} \exp\left(-\left(\frac{r}{r_R}\right)^{\alpha_R}\right), \tag{32}$$

where r_R is known as the Rosin–Rammler mean radius and α_R the Rosin–Rammler exponent. The Rosin–Rammler mean radius is the droplet radius for which 63% of the liquid mass is made up of droplets with smaller radii. The shape of the distribution is determined by the exponent, and the majority of sprays have distributions with exponents between the values of 2 and 4, and mostly at the lower end of this range, as reported by Wang and Lefebvre [19]. Thus the shape was chosen to match a Rosin–Rammler distribution of exponent 2. The number distribution found is

$$n(r) = \frac{16r}{r_{32}^2} \exp\left(-\frac{4r}{r_{32}}\right), \tag{33}$$

where the SMR r_{32} is used because all the droplet moments are defined in terms of the droplet radii, and it is not equal to the Rosin–Rammler mean radius. The comparison of the volume distribution produced by this approximation with the Rosin–Rammler distribution is made in Fig. 3.

The approach used is to consider the initial full distribution as a reference distribution based on a reference SMR which is invariant, and changes in the local SMR are obtained by truncating the distribution to match the SMR as predicted by the transport equations for Q_3 and Q_2. Values of SMR larger than the reference value are obtained by removing the small droplets from the distribution (Fig. 4), and SMR values smaller than the reference value are obtained by removing the large droplets from the distribution (Fig. 5). The other two moments can then be found from this truncated distribution. This model is equivalent to assuming that the change in the droplet size distribution is due to only larger droplets

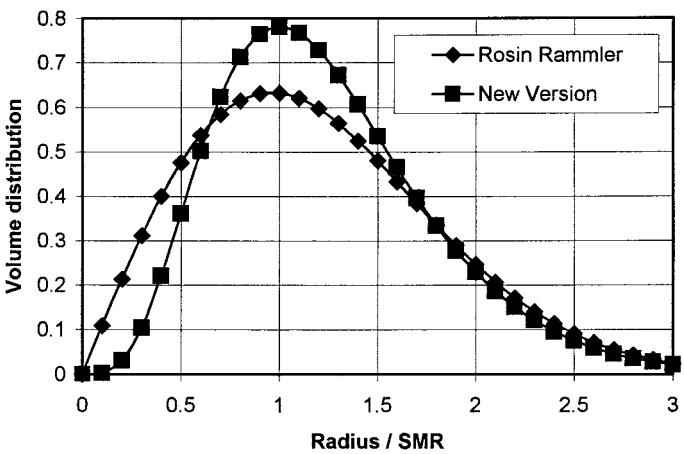

FIG. 3. Comparison of simplified distribution used in the model with the Rosin–Rammler distribution of exponent 2.

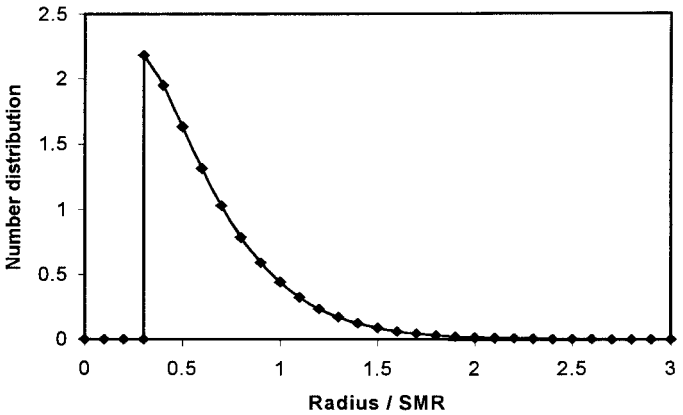

FIG. 4. Distribution truncated to remove small droplets when the calculated SMR is larger than the reference SMR.

being convected into some regions of the spray and only small droplets reaching other regions. The key reason for choosing this approach is that the truncated distribution tends towards having monodisperse behaviour, whichever end is being truncated. Therefore, once a certain droplet size is reached at the spray periphery, the moment-average velocities can be considered to be identical, and hence the instability problems can be completely solved. Details of the truncation procedure can be found in Beck [1].

3.3. *Interphase Drag*

This model provides the momentum transfer source term for the gas-phase momentum equation and both the moment-average liquid velocity equations. The change in the liquid momentum due to drag is given for a group, k, of droplets with identical properties as

$$\rho_l \gamma_k \frac{DU_{kj}}{Dt}. \tag{34}$$

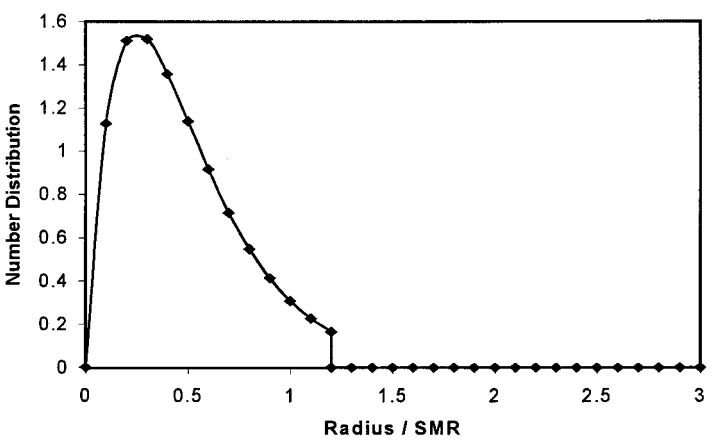

FIG. 5. Distribution truncated to remove large droplets when the calculated SMR is smaller than the reference SMR.

Integrating this over all droplets gives the total change in liquid momentum,

$$S_{U_{3j}} = \int_0^\infty \frac{4\pi}{3}\rho_l n(r) r^3 \frac{DU_j}{Dt}\, dr. \tag{35}$$

For the present version of the model, the radius-dependent Lagrangian derivative is given by

$$\frac{DU_j}{Dt} = \frac{3}{8}\frac{\rho_g}{\rho_l}\frac{|U_{rel}|}{r} C_d U_{rel,j}, \tag{36}$$

and the drag coefficient, which is also radius dependent, is given by the correlation of Wallis [20] for a solid sphere, where

$$\begin{aligned} C_d &= 0.424 && \mathrm{Re} > 1000, \\ C_d &= 24\left(\frac{1}{\mathrm{Re}} + 0.15\,\mathrm{Re}^{-0.313}\right) && \mathrm{Re} < 1000, \end{aligned} \tag{37}$$

and the Reynolds number is given as

$$\mathrm{Re} = \frac{2\rho_g |U_{rel}| r}{\mu_g}. \tag{38}$$

Other relations could be used in (36) and (37). These would affect the details of the derivations that follow, but not the substance.

One more key approximation is made in the modelling of this source term. The relative velocity between the liquid and the gas is taken to be constant with radius, with the value taken to be equal to the difference between the mass-average liquid velocity and the gas velocity. This assumption is justified by realising that the change in momentum of the spray as a whole locally is dominated by the changes in velocities of the large droplets, as these contain most of the spray momentum. The velocity of the large droplets is well approximated by the mass-average velocity. The added advantage of using this approximation is that it ensures that the liquid mass-average and gas velocities tend towards each other as the spray propagates downstream.

The Reynolds number of a droplet in a practical spray flow can only exceed 1000 in the near nozzle region in a very high pressure, high-speed spray, and hence droplets with Reynolds numbers over 1000 are not considered. The source term can now be written as

$$S_{U_{3j}} = \int_0^\infty \frac{\rho_g \pi}{2} n(r) r^2 |U_{rel}| U_{rel,j} \left(\frac{24\mu_g}{2\rho_g |U_{rel}| r} + 3.6\left(\frac{\mu_g}{2\rho_g |U_{rel}| r}\right)^{0.313}\right) dr. \tag{39}$$

Multiplying this out gives

$$S_{U_{3j}} = \int_0^\infty \left(6\pi n(r) r U_{rel,\,j}\mu_g + 1.8\pi \left(\frac{\mu_g}{2}\right)^{0.313} (\rho_g |U_{rel}|)^{0.687} U_{rel,j} n(r) r^{1.687}\right) dr. \tag{40}$$

Noninteger values of the radius are integrated by geometric interpolation between the surrounding moments. The right-hand side of these equation can now be integrated to give the final form of the source term:

$$S_{U_{3j}} = 6\pi\mu_g U_{rel,j} Q_1 + 1.8\pi(\rho_g |U_{rel}| Q_2)^{0.687} \left(\frac{\mu_g Q_1}{2}\right)^{0.313} U_{rel,j}. \tag{41}$$

A similar derivation is performed for the liquid surface-area average velocity source term. This time the source term is given by

$$S_{U_{2j}} = \int_0^\infty n(r) r^2 \frac{DU_j}{Dt}\, dr, \tag{42}$$

and the relative velocity used on this occasion is the difference between the surface-area-average velocity and the gas velocity. This again ensures that the surface-area-average velocity and the gas velocity tend towards each other as the spray propagates downstream. Inserting the models for the Lagrangian derivative and the drag coefficient, and integrating, gives the source term as

$$S_{U_{2j}} = \frac{9}{2}\frac{Q_0}{\rho_l} U_{rel,j}\mu_g + \frac{1.35}{\rho_l}(\rho_g |U_{rel}| Q_1)^{0.687} \left(\frac{\mu_g Q_0}{2}\right)^{0.313} U_{rel,j}. \tag{43}$$

3.4. *Droplet Breakup Model*

This model accounts for the effect on the droplet distribution function moments of the breakup of unstable droplets. There are generally considered to be three types of droplet instability (see, for example, Liu and Reitz [21]); they can undergo bag breakup, stripping breakup, and surface wave breakup. The last of these is mainly seen in the initial atomisation of the spray, and so the models described here only consider the other two. These models agree reasonably well with the thresholds determined by Nicholls [22], which are straightforward in nature and have been used in many DDM codes. The thresholds are

$$\mathrm{We} = \frac{\rho_g U_{rel}^2 r}{\sigma} = 6.0 \tag{44}$$

for bag breakup and

$$\frac{\mathrm{We}}{\sqrt{\mathrm{Re}}} = 0.5 \tag{45}$$

for stripping breakup. To break up, not only are the droplets required to reach these unstable threshold parameters, but also sufficient time is required. The breakup times used with the Nicholls parameters are

$$t_b = \pi \left(\frac{\rho_l r^3}{2\sigma}\right)^{\frac{1}{2}} \tag{46}$$

and

$$t_s = C_s \frac{r}{U_{rel}} \left(\frac{\rho_l}{\rho_g}\right)^{\frac{1}{2}}. \tag{47}$$

Nicholls took the constant C_s to be of order unity, but Reitz and Diwakar [23] argue that a value of 20 is suggested by empirical data. For the calculations presented in Section 5, $C_s = 1.0$ has been used and has been found to give good predictions of experimental data on drop sizes.

The correlation of [22] for stripping breakup (45) can be rearranged to give a critical radius, above which the droplets are unstable, by assuming that the droplets which are large enough to break are travelling at approximately the mass-average velocity. The critical radius can then be evaluated as

$$r_s = \frac{\sigma^2}{2\rho_g U_{rel}^3 \mu_g}. \tag{48}$$

Similarly, the critical radius above which bag breakup occurs can be written as

$$r_b = \frac{3\sigma}{\rho_g U_{rel}^2}. \tag{49}$$

Using these critical radii, and the fact that stripping breakup occurs in preference to bag breakup, the number of droplets potentially undergoing each type of breakup can be approximated by use of the assumed droplet size distribution function. The proportion of these droplets actually breaking up within a time step is given by

$$\frac{\delta t}{t_r}, \tag{50}$$

where δt is the time step and t_r is the time taken for an unstable droplet to breakup, as given for each breakup regime in (46) and (47) respectively.

The second, and much more difficult, aspect of modelling droplet breakup is to determine the results. Faeth *et al.* [24] use a physical argument to determine the resultant drop sizes, although they suggest that the value should be taken as a resultant Sauter mean diameter rather than the exact diameter of all droplets. This is based on the findings of Simmons [25] that the droplet size distribution produced by atomising droplets is characterised by a single distribution function moment, for example the SMR. The idea behind this model is that the drop sizes after breakup are related to the thickness of the laminar boundary layer of the droplet resulting from the motion of the droplet through the carrier gas, the similarity between the shear breakup of drops and the primary breakup of nonturbulent liquids having being noted by Hsiang and Faeth [26]. The validity of this model has been questioned by Liu and Reitz [27], whose experiments on drop breakup show that there is little dependence on the droplet Reynolds number. However, the correlation of [24] provides a useful starting point from which to build the outcome of the drop breakup within the context of the current methodology. Alternative formulations can easily be implemented in its place at a later date.

The correlation can be rearranged to give

$$r_{32,out} = 6.2\left(\frac{\rho_l}{\rho_g}\right)^{\frac{1}{4}}\left(\frac{\mu_l}{2\rho_l U_{rel}}\right)^{\frac{1}{2}} r_{in}^{\frac{1}{2}}, \tag{51}$$

which is valid for stripping breakup, the dominant form of breakup in the high-pressure sprays in which secondary breakup is important. Now, by assuming that the droplet volume is preserved in the breakup process (that is, there is no change in density and liquid mass is

conserved), the change in the second droplet moment due to the breakup of a single drop is given by

$$Q_{2,out} - Q_{2,in} = \frac{r_{in}^3}{6.2\left(\frac{\rho_l}{\rho_g}\right)^{\frac{1}{4}}\left(\frac{\mu_l}{2\rho_l U_{rel}}\right)^{\frac{1}{2}} r_{in}^{\frac{1}{2}}} - \frac{r_{in}^3}{r_{in}}. \tag{52}$$

For stripping breakup, the change in the surface area per unit time for a single droplet is given by dividing by the appropriate residence time for an unstable droplet, thus

$$S_{Q_2,s} = \frac{(Q_{2,s}\, Q_{1,s})^{\frac{1}{2}}}{6.2\left(\frac{\rho_l}{\rho_g}\right)^{\frac{1}{4}}\left(\frac{\mu_l}{2\rho_l U_{rel}}\right)^{\frac{1}{2}} \frac{C_s}{U_{rel}}\left(\frac{\rho_l}{\rho_g}\right)^{\frac{1}{2}}} - \frac{Q_{1,s}}{\frac{C_s}{U_{rel}}\left(\frac{\rho_l}{\rho_g}\right)^{\frac{1}{2}}}, \tag{53}$$

and $Q_{1,s}$ and $Q_{2,s}$ are the sum of radii and total sum of squares of radii undergoing stripping breakup.

For bag breakup, no appropriate correlation has been found in the literature, and so the surface area is assumed to double in the breakup, which is equivalent to the production of eight equally sized droplets. Thus

$$\frac{\delta Q_2}{\delta t} = \frac{r_{in}^{\frac{1}{2}}}{\pi\left(\frac{\rho_l}{2\sigma}\right)^{\frac{1}{2}}}. \tag{54}$$

Summing this over the appropriate droplets, and geometrically interpolating between the surrounding moments to integrate over noninteger powers of the radius, gives

$$S_{Q_2,b} = \frac{(Q_{0,b}\, Q_{1,b})^{\frac{1}{2}}}{\pi\left(\frac{\rho_l}{2\sigma}\right)^{\frac{1}{2}}}, \tag{55}$$

where $Q_{1,b}$ and $Q_{0,b}$ represent the sum of radii and total number of the droplets undergoing bag breakup.

These two contributions to the change in the surface-area droplet distribution moment are then summed to give the total change in the moment equation source term due to breakup. Note that these contributions to the S_{Q_2} source terms are also denoted as B_{Q_2} in Eq. (11) for surface-area-averaged momentum conservation. As this model only provides a value for the change in the Q_2 droplet moment, it is only appropriate for use when transport equations are being solved for only the Q_2 and Q_3 moments, with the other two being approximated from a presumed distribution.

3.5. *Droplet–Droplet Collision Models*

The collisions model is semiempirical and has three stages. The first stage is to determine the number of collisions between droplets occurring in any control volume. This is based on the collision frequency concept of O'Rourke and Bracco [28] that uses the assertion that the probability of n collisions between droplets in two different parcels in the same control volume in one time step can be modelled as a Poisson distribution, such that the probability is

$$P_n = e^{-\bar{n}}\frac{\bar{n}^n}{n!}, \tag{56}$$

where $\bar{n}$ is the average number of collisions, given by

$$\bar{n} = \frac{c\pi}{V_{cell}}(r_1 + r_2)^2 U_{rel}\delta t, \tag{57}$$

and the parcels contain droplets of radii $r_1 > r_2$. The number of droplets in the parcel with the smaller droplet diameter is denoted by c. A uniform random variable in [0, 1] is then used to determine whether a collision takes place. The probability of collision between two droplets per unit volume per unit time, providing they are in the same control volume, is then given by

$$p_{coll} = \frac{\pi}{V_{cell}^2}(r_i + r_j)^2 U_{rel}. \tag{58}$$

Since droplet parcels do not exist in the current methodology, an equivalent form involving the drop number distribution moments is required. This is obtained by multiplying the collision probability by the appropriate number distributions and integrating over all drops. In so doing each probability of collision is considered twice, so the number of collisions per unit volume per unit time is given by

$$N_{coll} = \frac{1}{2}\frac{\pi}{V_{cell}^2}\int\int (r_i + r_j)^2 U_{rel} n(r_i) n(r_j)\, dr_i\, dr_j. \tag{59}$$

In this equation U_{rel} is a function of r_i and r_j. However, the form of this function is not known, hence, to date in the model it has been approximated by assuming a mean relative value between all colliding drops. With this assumption

$$N_{coll} = C_{coll}\pi \bar{U}_{rel}\left(Q_0 Q_2 + Q_1^2\right), \tag{60}$$

where the power of V_{cell} is reduced by 2 because the Q_i measure the droplet moments per unit volume. C_{coll} is a model constant introduced due to the prediction of large numbers of collisions with this model. It is usually taken as 0.15, as discussed in Section 4. The relative velocity between droplets is approximated by assuming that the large droplets are travelling at approximately the mass-average velocity and that the small droplets have been fully entrained to the gas velocity. This means that the average droplet–droplet relative velocity is approximated as one-half of the relative velocity between the mass-average liquid velocity and the local gas velocity. The need to model the average relative velocity is not required in Lagrangian models and can be considered a weakness of using an Eulerian approach. This is the likely reason for the need of the model constant C_{coll}, which is not used in Lagrangian models.

The second stage of the model determines how many of these collisions result in each of the regimes of coalescence, bounce, and separation described by Orme [29]. The two parameters required to determine these proportions are the Weber number, defined as

$$\mathrm{We} = \frac{2r\rho_l \bar{U}_{rel}}{\sigma}, \tag{61}$$

and the impact parameter b. The impact parameter is defined as the perpendicular distance from the centre of one droplet to the relative velocity vector placed on the centre of the other droplet at impact, normalised by the sum of the radii. This is illustrated in Fig. 6.

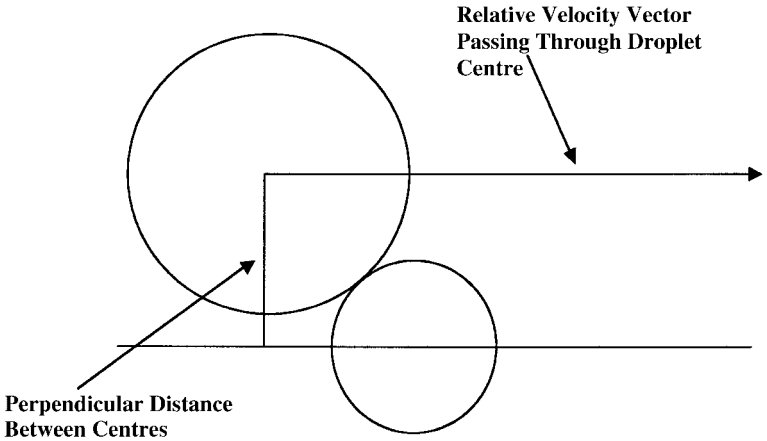

FIG. 6. The perpendicular distance between centres at impact as used in the impact parameter definition.

Jiang *et al.* [30] provide a map of the different regimes on a graph of Weber number against impact parameter, which is presented here as Fig. 7. This chart is for hydrocarbon droplets and is simplified for the model and taken to be that presented as Fig. 8. It is worth noting that the thresholds between regimes are slightly dependent on the ambient pressure. The chart used is based on an ambient pressure of 0.1 MPa.

The critical Weber numbers shown on the chart are now translated into critical radii (as in the breakup model), and an assumed distribution is used to determine the probability that any given droplet lies between adjacent critical radii. The outcome of a collision is decided by the Weber number of the *smaller* droplet, according to [29], and the impact parameter. For the hydrocarbon droplets, there exist three critical radii, and the probability that the smaller radius of the two colliding droplets falls between given critical radii is given by

$$P(r_{smaller} < r_a) = P(r < r_a)(2 - P(r < r_a)), \tag{62a}$$

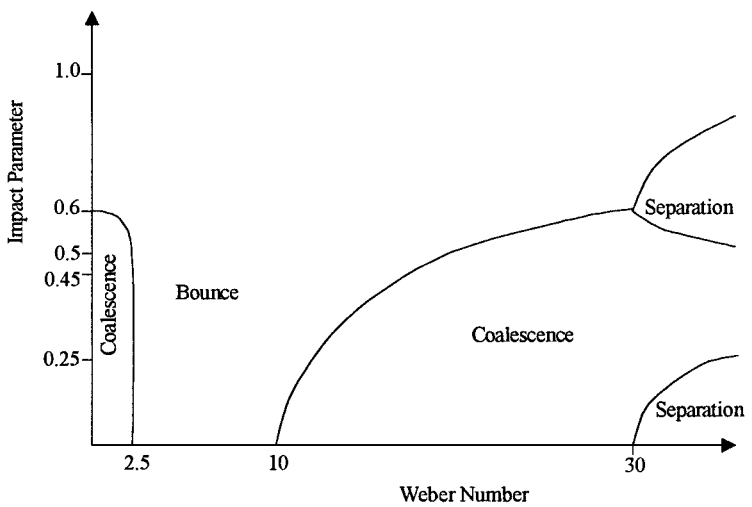

FIG. 7. Transition criteria between regimes of collision between hydrocarbon droplets. Adapted from Jiang *et al.* [30].

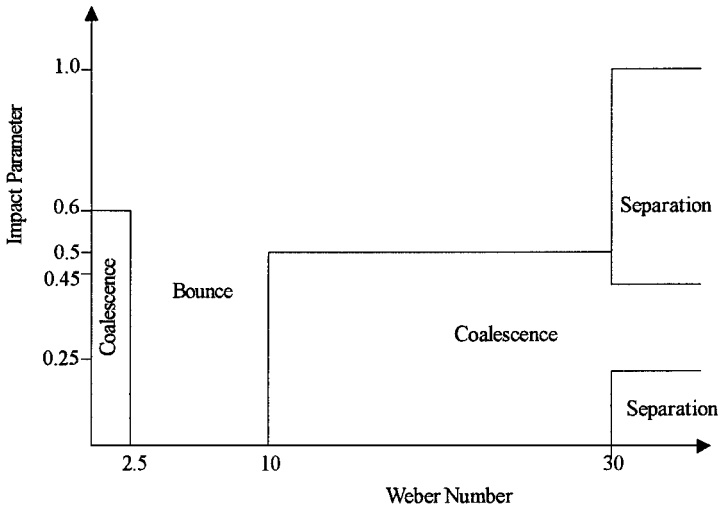

FIG. 8. Simplified schematic of collision regimes transition criteria for hydrocarbon droplets as used in the model for determining the probability of each occurring.

$$P(r_b < r_{smaller} < r_c) = P(r_b < r < r_c)(P(r_b < r < r_c) + 2P(r > r_c)), \tag{62b}$$

$$P(r_{smaller} > r_c) = P(r > r_c)^2, \tag{62c}$$

by considering the sizes of the two droplets as independent events. These values are given by summing the probability of the first droplet being in the desired radius range and the second droplet being at least this size and the probability that the second droplet is in the desired radius range with the first droplet being in a larger radius range. The probability of the smaller droplet falling between r_a and r_b is not of interest in this case as these droplets undergo bounce. The collisions undergoing the bounce regime can be ignored in this model because the total mass, surface area, and momentum of the liquid are conserved during a bounce collision, and hence there is no net change to any of the spray parameters considered in the model.

Modelling the impact parameter as a uniform random variable on [0, 1], as all values are equally likely, acts to determine what proportion of the collisions occurring with the smaller droplet between given critical radii result in each collision regime. Thus Fig. 8 shows that where the smaller droplet has radius less than r_a the probability of a collision resulting in coalescence is 0.6, and the probability of a bounce collision is 0.4. In the same way the probabilities of the coalescence and separation regimes given the radius of the smaller droplet can be approximated. The values are given in Table I.

TABLE I

Probabilities of Collision Outcome for Hydrocarbon Droplets Given the Radius of the Smaller Droplet

	P_{coll}	P_{sep}
$r_{smaller} < r_a$	0.6	0
$r_b < r_{smaller} < r_c$	0.5	0
$r_{smaller} > r_c$	0.2	0.8

TABLE II
Determination of Surface Area Change for Collisions between Hydrocarbon Droplets

	Initial droplet size, r_{in}	Change in square of radius
$r_{smaller} < r_a$	r_a	$\delta Q_{2,a} = (2^{2/3} - 2)r_{in}^2 = -0.41r_{in}^2$
$r_b < r_{smaller} < r_c$	$0.5(r_b + r_c)$	$\delta Q_{2,b} = (2^{2/3} - 2)r_{in}^2 = -0.41r_{in}^2$
$r_{smaller} > r_c$ (coalescence)	r_c	$\delta Q_{2,c} = (2^{2/3} - 2)r_{in}^2 = -0.41r_{in}^2$
$r_{smaller} > r_c$ (separation)	r_c	$\delta Q_{2,sep} = (5 \cdot (0.4)^{2/3} - 2)r_{in}^2 = 0.71r_{in}^2$

Hence the total coalescence probability for hydrocarbon droplets can be given as

$$P_{coal} = P_{coal,a} + P_{coal,b} + P_{coal,c}, \tag{63}$$

where

$$P_{coal,a} = 0.6P(r < r_a)(2 - P(r < r_a)), \tag{64a}$$

$$P_{coal,b} = 0.5P(r_b < r < r_c)(P(r_b < r < r_c) + 2P(r > r_c)), \tag{64b}$$

$$P_{coal,c} = 0.2P(r > r_c)^2 \tag{64c}$$

are the probabilities of a collision with the smaller droplet between each set of critical radii. The probability of separation is more straightforwardly

$$P_{sep} = 0.8P(r > r_c)^2. \tag{65}$$

The final stage of the collisions model is to determine the effect of the predicted collisions on the droplet moments, specifically the surface area, as the liquid mass is conserved during the collision. The surface area change is considered to be approximated by that obtained from a collision between two droplets of equal radius and to result in either one (coalescence) or five (separation) droplets, also of equal radius, such that the droplet volume is conserved. The effect of changing the number of droplets produced in separation has not been tested. The radius of the drops entering the collision, r_{in}, is dependent on the Weber number, and the values it takes for each regime are presented in Table II for hydrocarbon droplets, along with the change in the square of the radius, δQ_2, resulting from the collision.

Hence the final source term for the surface area moment is

$$S_{Q_2,coll} = N_{coll}(P_{coll,a}\delta Q_{2,a} + P_{coll,b}\delta Q_{2,b} + P_{coll,c}\delta Q_{2,c} + P_{sep}\delta Q_{2,sep}), \tag{66}$$

where the P_{coll} derived here are for hydrocarbon droplets. Similar equations and tables have been produced by Beck [1] for water droplet collisions.

4. COMPUTATIONAL SCHEME

4.1. *Introduction*

This section presents an outline of the implementation of the mathematical framework described in the previous sections into a finite-volume computational model. Of particular interest here is the way in which the liquid-phase equations are treated and incorporated

TABLE III
Values of X, ρ, S_L, U_j, Γ_Φ Used in each Transport Equation

Equation, Φ	X	ρ	S_L	U_j	Γ_Φ
Liquid phase mass average velocity, U_{l3}	$1-\theta$	ρ_l	S_m	U_{l3j}	$\rho_l \sigma_v \nu_1$
Liquid phase surface area velocity, U_{l2}	Q_2	1	S_{Q_2}	U_{l2j}	$\sigma_v \nu_1$
Liquid volume, Q_3	1	ρ_l	0	U_{l3j}	0
Liquid surface area, Q_2	1	1	0	U_{l2j}	0
Gas phase continuity, 1	θ	ρ_g	0	U_{gj}	0
Gas phase momentum, U_g	θ	ρ_g	$-S_m$	U_{gj}	μ_{eff}
Turbulence energy, k	θ	ρ_g	$-S_m$	U_{gj}	μ_{eff}/σ_k
Turbulence energy dissipation rate, ε	θ	ρ_g	$-S_m$	U_{gj}	$\mu_{eff}/\sigma_\varepsilon$

into an existing single-phase solution scheme. The manner in which the transport equations are discretised is discussed in Section 4.2. Section 4.3 presents the PISO-based solution algorithm.

4.2. *Discretisation*

The equations being solved fall into three categories, the gas-phase transport equations, the liquid-phase transport equations, and the droplet moment equations. All these equations can be written in the general form

$$\frac{\partial}{\partial t}(X\rho\Phi) + \frac{\partial}{\partial x_j}(X\rho\Phi U_j) + \Phi S_L = \frac{\partial}{\partial x_j}\left(X\Gamma_\Phi \frac{\partial \Phi}{\partial x_j}\right) + S_\Phi. \tag{67}$$

The values taken for the variables X, ρ, S_L, U_j, and Γ_Φ for each equation are listed in Table III. S_Φ is the relevant source term as derived in Sections 2 and 3.

This general transport equation is then discretised in a finite-volume framework. It is integrated over a control volume and a time interval δt. This is a standard procedure that has been presented many times before for single-phase flow calculations (see, e.g., Versteeg and Malalasekera [31]) and so will not be presented in detail. However, the approaches used are outlined here.

The equations are all solved on the same two-dimensional, axisymmetric, orthogonal computational grid. The backward staggered grid approach is used, which involves defining a central control volume for the gas pressure and other scalar variables, including the moments Q_2 and Q_3, and displaced volumes for the gas and liquid velocities. This has the advantage of strongly coupling the gas velocity and pressure and also results in the ability to check continuity for both phases over the central volume without the need for interpolation.

The temporal differencing is performed using the Euler implicit discretisation method. This results in a fully implicit scheme that allows larger time steps to be taken before the scheme becomes unstable. This is generally a good idea in the modelling of spray flows, as a fine grid is required around the nozzle region to resolve the large dependency on inlet conditions. An explicit scheme, for stability, requires prohibitively small time steps. This is especially the case when considering the large injection velocities of high-pressure diesel sprays.

Spatial discretisation of the velocity equations for both phases and the turbulence model equations is done using the hybrid scheme of Spalding [32]. This involves using a second-order-accurate central-differencing scheme for computational cells with low

Reynolds numbers and a first-order upwind scheme for cells with high Reynolds numbers. This enhances stability, as the central differencing scheme is unstable at high Reynolds numbers, but results in numerical diffusion. This is a very simple and not especially accurate differencing scheme. It has been used mainly for its simplicity and robustness, as the major part of the work being done is the design of equations that can adequately model the physics of sprays. The moment equations, which lack a second-order diffusion term, are treated using the first-order upwind scheme. The gas-phase continuity equation is not solved directly. Instead it is used, along with truncated forms of the gas-phase momentum equations, to form pressure-correction equations. These, when solved, determine corrections to the gas-phase pressure, density, and velocity components. The details of this process, embodied within the PISO algorithm, are given by Issa [33]. The liquid-phase momentum equations do not need this procedure, because they lack the pressure-gradient source term.

4.3. *Solution Algorithm*

The solution algorithm is based on the PISO algorithm of Issa [33], with the liquid-phase equations added into it. A key feature of the amended algorithm is that the spray solution is obtained first, and then the reaction of the gas phase is calculated. This is the natural way to proceed given the dominance of the spray in determining the flow field.

The PISO algorithm provides an efficient noniterative solution procedure that couples the gas-phase pressure and velocity components by an operator-splitting technique and solves the equations of motion for the gas phase in a predictor–corrector fashion. The current scheme solves the liquid equations only once, at the beginning of the time step. Use of corrector equations was tested [1], but it was found that the corrections obtained in the corrector steps were very small. It was decided that the computational time saved in solving the liquid equations only once in a time step was of greater benefit in comparison with a very slight increase in accuracy. The stability of the scheme was unaffected.

The use of a noniterative scheme implies that some effects are lagged, i.e., carried forward from one time step into the next. In the current approach, the droplet breakup and collision effects are calculated at the end of the time step, and the amended source terms for the Q_2 equations and for the surface-area-averaged momentum equations are therefore carried forward to the beginning of the next time step.

The solution proceeds in the following manner:

Step 1: Droplet size distribution moment transport equations. The transport equations (8) and (9), for the moments Q_2 and Q_3 of the droplet size distribution function, are solved. The void fraction is updated. Moments Q_0 and Q_1, requiring approximation from the assumed distribution function, are calculated.

Step 2: Drag equation. The interphase drag source terms, Eqs. (41) and (43), are evaluated.

Step 3: Liquid-phase momentum equations. The transport equations (10) and (11), for the moment-average velocities U_{l2} and U_{l3}, are solved.

Step 4: Bulk adjustment. During spray injection, the volume available to the gas changes due to some of the space now being filled with liquid. This effect is only appreciable in the near-nozzle region. Nevertheless, a bulk adjustment is incorporated into the algorithm to account for this, as it is relatively inexpensive. The gas-phase pressure and density are updated.

Step 5: Gas-phase momentum prediction. The gas-phase velocity components are predicted using the gas-phase momentum transport equations (13).

Step 6: First gas-phase momentum corrections. The first set of pressure-correction equations are solved (see [1] and [33] for details). The gas-phase pressures, densities, and velocity components are corrected.

Step 7: Second gas-phase momentum corrections. The second set of pressure-correction equations are solved. The gas-phase pressures, densities, and velocity components are corrected again.

Step 8: Gas-phase turbulence equations. Transport equations (15) and (16) are solved for the turbulence kinetic energy and its dissipation rate. The equations are coupled and iterated to convergence.

Step 9: Source term calculation for droplet dynamic effects. The effects considered here are the breakup of unstable droplets and collisions between droplets. As detailed in Section 3, source terms are provided for the effect of each of these phenomena on the Q_2 transport equations and on the surface-area-averaged momentum equations.

The stability and robustness of this scheme has been demonstrated by the ability of the method to obtain converged solutions of the equations for all the test cases that have been attempted to date [1–3, 10]. The accuracy of the method has been partially assessed in these publications and is further assessed in the following section of this paper, by comparisons with experimental data on spray penetration and drop sizes for a number of test cases.

5. TEST CASES

5.1. *Introduction*

High-pressure, narrow-angle sprays have high injection velocities and spray penetration results are often quoted, allowing assessment of the momentum transfer model. Also, the high velocities result in much secondary breakup, thus testing the breakup modelling, and the narrow sprays are relatively dense, resulting in enough collisions to validate the collisions model. These sprays are strongly one dimensional, and the droplet sizes found at different downstream distances are dependent mainly on breakup and collisions and are thus a good indicator of the model performance.

The cases chosen for the submodel tests are the sprays of Hiroyasu and Kadota [34], the physical conditions for which are given in Table IV. Penetration results, measured photographically, and the spray SMR at 65 mm downstream from the nozzle, averaged over axial spray cross sections, are given by the experiments; hence, the computational tests

TABLE IV
Test Conditions for the Data of Hiroyasu and Kadota [34]

	Case H1	Case H2	Case H3
Ambient pressure (MPa)	1.1	3.0	5.0
Spray angle	10°	16°	21°
Injection velocity (m s^{-1})	102.0	90.3	86.4
Droplet SMR at 65 mm (μm)	21.2	24.5	29.4
Injection pressure (MPa)	9.9	9.9	9.9

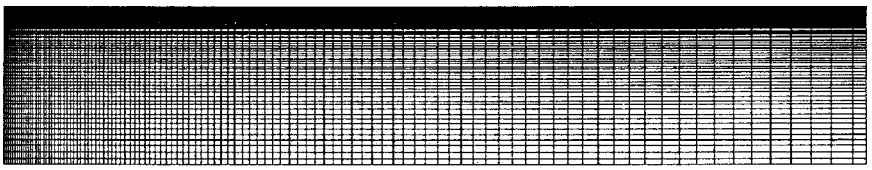

FIG. 9. Grid used for the Hiroyasu and Kadota [34] test cases. The domain is 200-mm long and 37 mm in radius with 109×73 cells.

will consider these same variables. The cross-sectional average Sauter mean radii given in the computations are instantaneous values after 12 ms. Unfortunately, there is no precise definition of the spray tip in either computation or experiment. Probably the most sensible definition of the spray tip is the point behind which 99% of the spray mass is located. This definition will be used throughout the work done on solid cone sprays. These test cases have also been modelled, using a DDM scheme, by Reitz and Diwakar [23] and others, providing a useful comparison with the results obtained by the new model.

For the present comparisons, a time step of 2 μs has been used. The maximum dimension of the injection cell is 0.5 mm, in a 109×73 line grid, as shown in Fig. 9, and the droplets have an inlet SMR and reference SMR of 20 μm in all cases. The spray cone angles were estimated using the correlation of Ranz [16], and the diesel fuel has density 840 kg m^{-3}.

For this model to be considered a widely applicable spray model, its performance in the simulation of hollow-cone sprays must be tested. In particular, is the physics of the spray described well enough in the model such that the change of computational injection scheme discussed in Section 3.2 is sufficient for an accurate simulation of a hollow-cone spray? Entrainment of a central gas jet where there are very few droplets (due to the hollow nature of the spray) and successful capture of the collapse of the cone as indicated by spray width data are of particular interest.

The definition of spray penetration is taken to be slightly different in this case because the spray tip does not necessarily travel in an approximately straight line as in a solid-cone spray. Hence the spray tips are much less densely populated and so the forwardmost 1% of the mass occupies a significant part of the spray volume, stretching well back from the spray tip. To gain meaningful results in this case, a useful definition for the spray tip is the axial distance beyond which 1000 droplets are located. Similarly, the spray width is calculated as the radial distance beyond which 100 droplets are located. The droplet numbers are obtained using the values of Q_0. The choice of different numbers of droplets to measure each dimension reflects the fact that the spray tip is more densely populated than the spray edge.

The data used for comparison are those of Ren and Nally [35], who injected an *n*-heptane spray using a pressure-swirl atomiser into air of different ambient pressures. Data were obtained photographically for the spray penetration and the spray width over the first 2 ms. The conditions for the experiment are given in Table V.

For the calculations, the time step used is 1 μs, and the injection cell has a maximum side of length 0.5 mm. An inlet droplet SMR equal to the reference SMR of 15 μm is used. The injection velocity and inlet sheet thickness were taken equal to the quoted values. The injection pressure was 7.0 MPa, the spray thickness angle was calculated from the correlation of Ranz [16], and the nozzle has a radius of 0.45 mm. The grid used is the same as for the narrow-cone cases, shown in Fig. 9, except that the domain is stretched in the radial direction to 80 mm to accommodate the wide-angle spray.

TABLE V
Conditions for the Experiments of Ren and Nally [35]

	Case R1	Case R2	Case R3
Ambient pressure (MPa)	0.1	0.45	0.93
Injection velocity (m s^{-1})	37.7	37.7	37.7
Nominal cone angle	80°	80°	80°
Spray thickness angle	3.3°	7.0°	10.1°
Sheet thickness at injector (μm)	195	195	195

5.2. *Comparison with Experiment*

Penetration results for narrow-cone sprays are presented as Fig. 10. Excellent agreement can be seen between the experimental and computational results. Although penetration is controlled by turbulence diffusivity, an accurate momentum transfer model is vital in determining the predicted spray penetration. The use of the truncation approximation to approximate the droplet size distribution and droplet moments is also supported as the momentum transfer model is dependent on the values of all four moments. Clearly the predicted values of the moments and momentum transfer must be acceptable for the model to be able to produce penetration results of this accuracy. Figure 11 compares the droplet SMR values predicted by the model with those predicted by Reitz and Diwakar [23] using the DDM. The different treatment of the injection conditions makes comparisons between the droplet sizes meaningless until the end of the breakup zone is reached. Hence results are presented from 40 mm downstream of the nozzle. Also included in the figure is the experimental result of Hiroyasu and Kadota [34] at 65 mm downstream of the injector. The predicted increase in the droplet sizes with increasing ambient density agrees with both the DDM and the experimental results. Similar droplet sizes are predicted at 40 mm downstream of the nozzle in both models, suggesting that the breakup models employed in each are behaving comparably and the coalescence of droplets then takes over as the

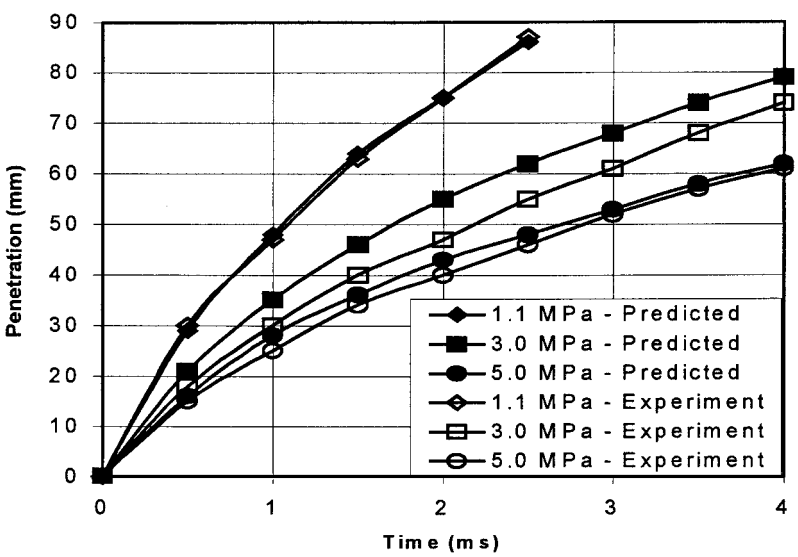

FIG. 10. Spray penetration results for the test cases of Hiroyasu and Kadota [34].

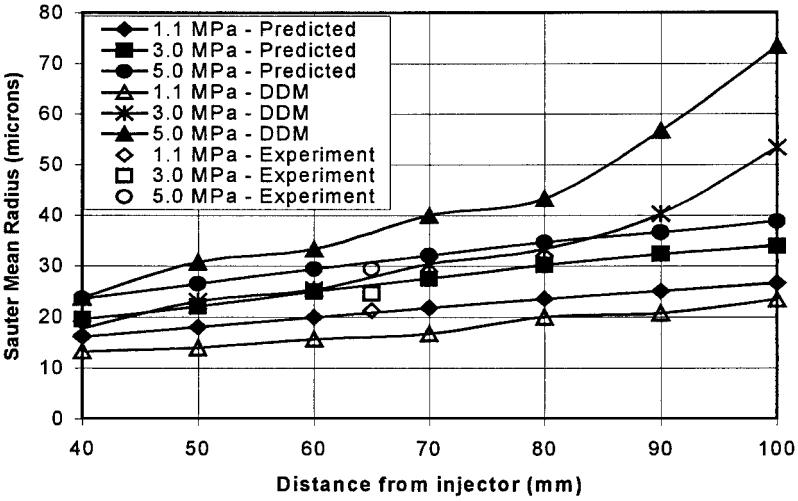

FIG. 11. Droplet SMR results for the test cases of Hiroyasu and Kadota [34].

dominant factor in the determination of the SMR in both models. One valuable advantage of the new model is its ability to give instantaneous values of the SMR at any location at any time, but the DDM relies on collecting data on passing droplets over a period of time, in this case 10 ms.

The penetration results for the hollow-cone cases are presented in Fig. 12. Reasonable agreement can be seen between the predictions and the experiments, although not to the quality seen in the narrow-angle spray results. In the very initial stages of injection the penetration is severely overpredicted as in reality it takes the hollow-cone structure some time to form, whereas it is assumed to form immediately in the computation. By 1 ms the agreement is much better, and it remains so until 2 ms. Overall the results are good and the momentum transfer model and predicted spray structure are well validated. The spray width results shown in Fig. 13 are also reasonable, although poorer than the penetration results. Again the real spray forms less quickly than the predicted spray, although the spray

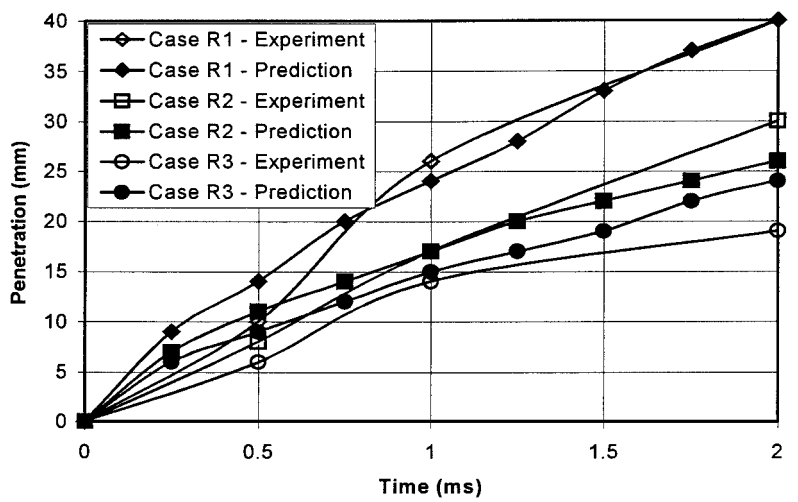

FIG. 12. Comparison of predicted spray penetration with the experimental data of Ren and Nally [35].

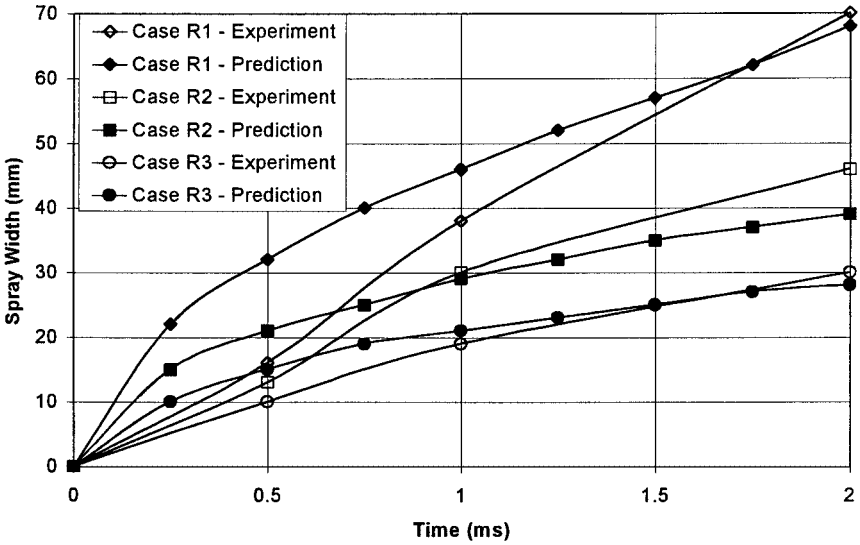

FIG. 13. Comparison of predicted spray width with experimental data of Ren and Nally [35].

width results become more accurate after the first millisecond. The rate of increase of spray width is underestimated at 2 ms, so it is likely that the spray width will be slightly underpredicted at later times, possibly due to the entrainment of too much gas. An overall SMR is quoted in [35] for the spray as 13.6 μm for case R1. This is reasonably close to the predicted size results of Fig. 14.

5.3. *Effects of Submodels*

Figure 15 shows the effect of including the breakup and collisions models on the prediction of the spray droplet sizes in the narrow-cone baseline case H1. It can be clearly seen that all changes in droplet SMR between 30 and 100 mm downstream of the nozzle are

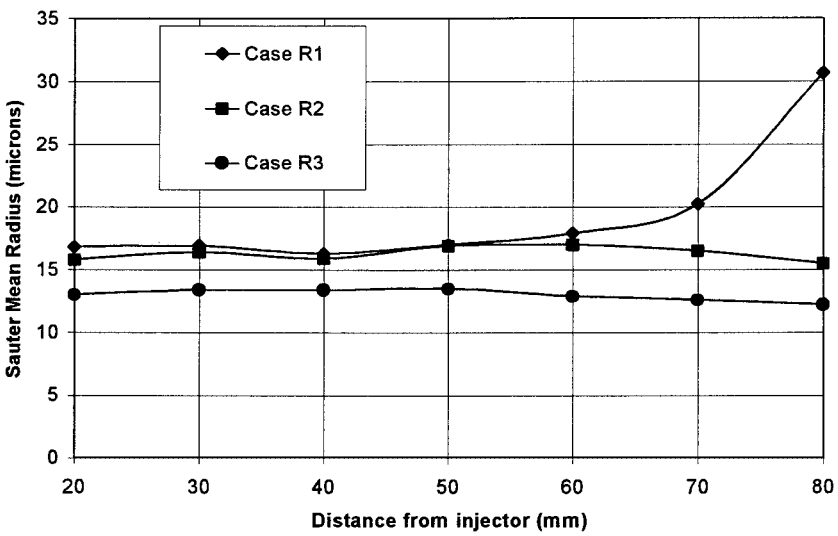

FIG. 14. Variation in Sauter mean radius with ambient pressure.

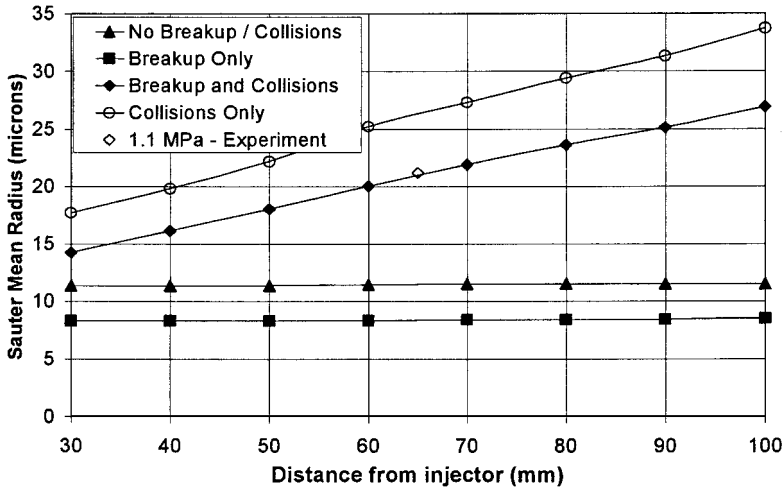

FIG. 15. Droplet sizes produced by droplet dynamic models for test case H1.

caused by these two phenomena. The effect of breakup is to reduce the droplet SMR in the near-injector region, and coalescence between droplets causes the increase in the droplet SMR as the axial distance increases.

The effects of the breakup and collisions models on the drop sizes in the hollow-cone spray for case R1 are presented in Fig. 16. The droplet SMR growth rate with downstream distance is very small beyond 20 mm from the injector whether collisions are accounted for or not. Thus it can be concluded that collisions are only important in the very near nozzle region. The inclusion of the droplet breakup model has very little effect on the downstream droplet SMR values, which suggests that very few droplets introduced at inlet are aerodynamically unstable in this spray flow.

The prediction of larger drops in the near-orifice region when collisions are accounted for results in some variation in the hollow-cone spray shape. As shown in Fig. 17, the spray

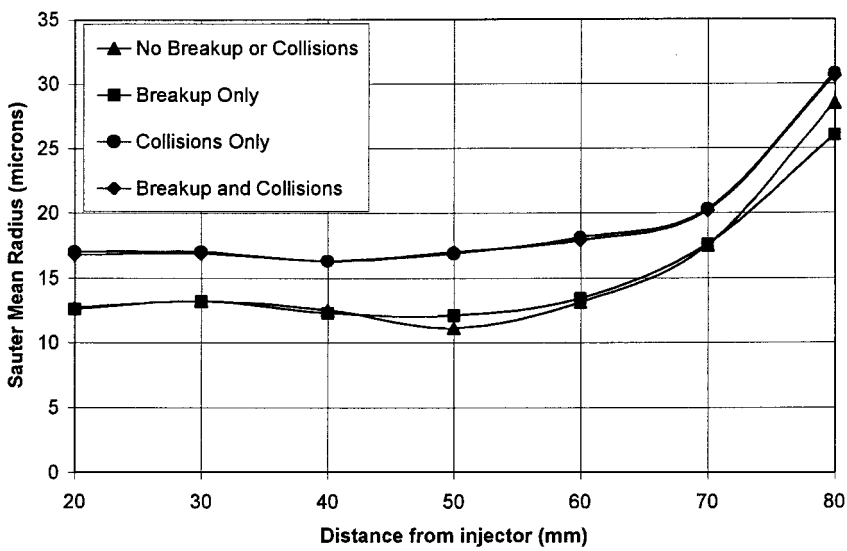

FIG. 16. Effect of droplet dynamic models on Sauter mean radius for test case R1.

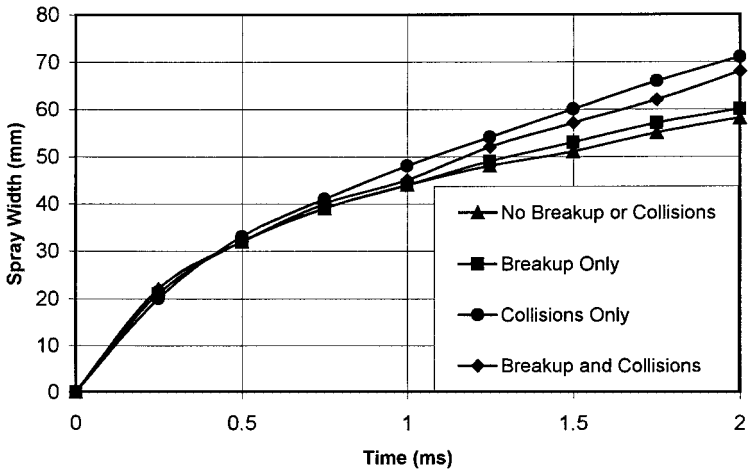

FIG. 17. Effect of droplet dynamic models on spray width for test case R1.

is predicted to be significantly wider, and the axial penetration also increases by a lesser amount, due to the smaller effect of drag on the larger drops.

The collisions source term contains a model constant (see Eq. (60)) and therefore the effects of this constant on the spray predictions require investigating. Figure 18 shows the effect of increasing the constant on the droplet sizes for the narrow-cone case H1. This figure confirms that coalescence is the dominant result of the collisions. The recommended value of the constant is 0.15, as this gives predictions of drop sizes that match the experimental value at 65 mm, and this value is used in all other calculations. It should also be noted that the droplet sizes at the 30-mm axial distance do not increase rapidly with the collisions constant. This suggests that in the near-injector region the effect of droplet breakup is dominant over the effect of droplet coalescence. The collision regime predicted in this region by the model is the fragmentation regime due to the much higher relative velocities between droplets.

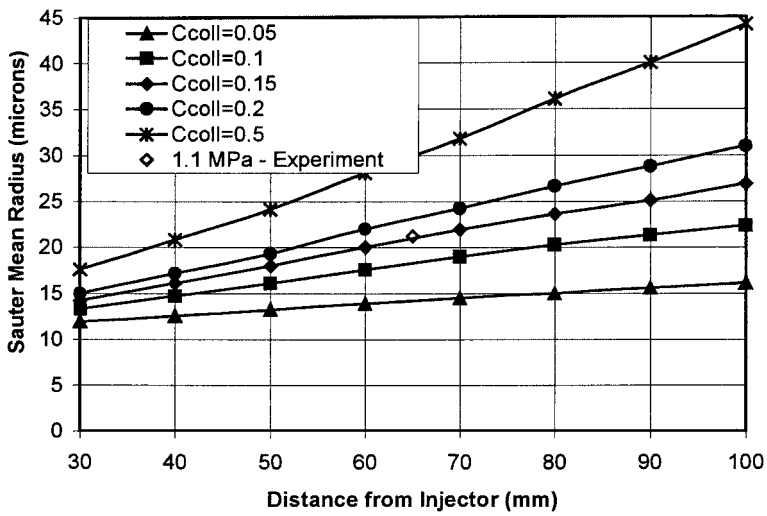

FIG. 18. Variation of droplet sizes with collisions coefficient for test case H1.

Because of the relatively few collisions occurring in hollow-cone sprays, this constant has little impact on the drop size predictions for that class of spray.

5.4. *Numerical Effects*

Both the spray penetration and droplet size results for all cases show good insensitivity to the time step used, for a range of step size from 0.5 to 2.0 μs. The largest effect is seen on the penetration of narrow-cone sprays, where a maximum variation of about 5% is found after 3 ms of injection [1].

The effect of the grid on the results was measured by changing the size of the injection cell and the rest of the grid proportionally. The injection cell size was based on the maximum dimension of the cell (always in the axial direction), which ranged from 0.3 to 2 mm in these tests. The number of cells ranges from 180×120 to 27×18. For the narrow-cone spray cases the predicted penetration is almost unaffected as the grid is coarsened, with a maximum variation of about 8% [1]. The coarse grids used with DDM models cause the gained gaseous momentum to be spread over too large a gas volume; hence the velocity difference between the phases is maintained at too high a level and the remaining drag force is overpredicted as a result, causing low values of the spray penetration (Abraham [36], Watkins and Khaleghi [37]). However, even the coarsest grid size used here is sufficiently fine to allow the scheme to predict the localised gas entrainment created by disperse droplets.

The smallest downstream SMR values in narrow-cone sprays are predicted when using the coarsest grid [1]. This is due to the large cells at the centreline not capturing the full thickness of the spray, and hence this more dilute picture of the spray results in fewer droplet collisions and thus smaller downstream SMR values. Even then the maximum variation in drop sizes using these grids is only about 10%. The results obtained differ very little for both penetration and droplet sizes using the two finest grids, showing a good degree of grid independence.

The penetration results obtained for hollow-cone spray case R1 using four different grids are shown on Fig. 19. Very good agreement is seen between the results produced by the three finer grids, with the coarsest grid overpredicting the penetration. Similar agreement between the three finer grids is found in the prediction of the spray width [1]. The coarse grid overpredicts the width initially due to the large cell size, and eventually it underpredicts

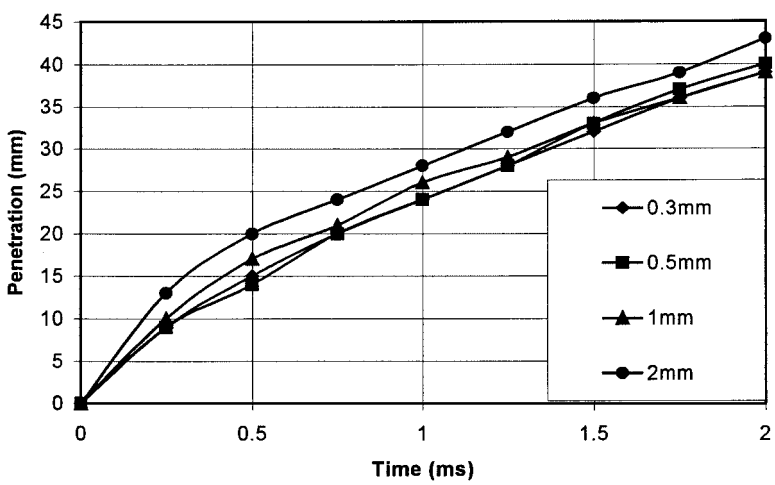

FIG. 19. Variation in spray penetration with computational grid density, measured in terms of the longest side of the injection cell, for test case R1.

the width. This is caused by the prediction of too much spray collapse, which also causes the overprediction of penetration to continue beyond the initial stages of injection. As with the narrow-cone spray, the droplet SMR reduces as the grid becomes coarser due to the prediction of fewer collisions near to the injector in coarse grids. In most of the spray, there is little change in droplet size, and so the predicted sizes do not differ a great deal from each other. The sizes predicted by the two finest grids are very similar, showing that there exists a high degree of grid independency among these results [1].

6. CONCLUSIONS

The spray model, extended and applied in this work, has been developed in previous publications [1, 2]. The model uses the moments of the droplet number distribution as the parameters required to construct a polydisperse Eulerian spray model that does not require droplet size classes. Transport equations were developed for two of these moments involving the use of suitable moment-average velocities, and two further moments were obtained from a suitable number distribution function. Transport equations have also been derived for the moment-average velocities where required.

In this paper submodels have been designed to capture the effects of interphase drag, droplet breakup, and droplet–droplet collisions. Parametric tests have shown that the spray performance is physically consistent, with a small dependence on time step and grid density. The test cases employed in the previous publications, and the work presented here, show that the model can use much finer grid spacings than a DDM, resulting in smaller numerical errors. The model produces excellent spray penetration results in comparison with experimental data, thus supporting the interphase transfer models. The collapse of the hollow cone is also evident in the predictions, in good agreement with experimental data.

The model has been applied here to calculate local values of the drop sizes produced by narrow-cone and hollow-cone sprays. The results predicted are in good agreement with experimental data. The performance of the breakup and collisions models in dense narrow-angle sprays is supported by good predictions of droplet sizes.

The present method is believed to be computationally inexpensive. Beck and Watkins [38] quote CPU times required to predict narrow-cone sprays using the same grid density as applied in the test cases here. Low-injection-pressure cases (17 MPa), using a time step of 2 μs, required less than 5 minutes of CPU time on a Sun Enterprise 450 workstation. With higher injection pressures of 137 MPa, requiring a time step of 0.2 μs, the CPU time was 40 minutes. No direct comparisons with a DDM have been undertaken.

The model has successfully predicted the main features of the spray, but there are aspects of the model in which improvements can be made. One area that has not been investigated yet is the possibility of constructing a primary atomisation model where large blobs of liquid are inlet at the injector and are shattered into small droplets. This could be achieved in the model via a droplet breakup source term for Q_2. This has the potential to better capture phenomena such as the breakup length and predict the very small droplet sizes seen in high-pressure sprays.

Only one assumed number distribution has been used in the course of this work. Future work should consider a number of analytically integrable functions and compare the behaviour of the model with different assumed distributions, as it is known that different atomisers produce different droplet size distributions. Comparing the local distribution as well as the SMR with experimental data would also provide insight into the behaviour of

the model and provide a practical basis for deciding how to change the assumed droplet size distribution with space and time.

Recent studies of wall impaction [39, 40] have shown that the results of modelling attempts that consider groups of single droplets have not provided satisfactory results in comparison with experiment. Roisman *et al.* [40] concluded that the impact of a polydisperse spray cannot be described by the linear superposition of single droplet impacts, and they define an average Weber number at impact to correlate the droplet diameter distribution after impact. This use of average properties and distribution correlation suggests that these could be fairly straightforwardly introduced into the present model to predict spray–wall impaction. Average spray quantities could be defined in terms of the droplet moments and moment-average quantities to determine the postimpingement spray characteristics, i.e., the resultant droplet moments and moment-average quantities. To obtain useful correlations for the postimpingement characteristics, it is likely that this will be done in a mainly empirical manner using as wide a range of different impaction conditions as possible.

APPENDIX: NOMENCLATURE

b	Impact Parameter
B_{Qi}	Source Term due to Breakup
c	Number of Drops
C_{coll}	Collision Constant
C_D	Discharge Coefficient
C_d	Drag Coefficient
C_s	Breakup Time Constant
C_μ, $C_{\varepsilon 1}$	
$C_{\varepsilon 2}$, $C_{\varepsilon 3}$	Turbulence Parameters
D	Diameter
H	Injection Cell Length
h	Liquid Sheet Thickness
k	Turbulent Kinetic Energy
N	Number of Drops
N_{coll}	Number of Collisions
$n(r)$	Number Size Distribution
P	Pressure
p	Partial Pressure, Probability
P_k	Production of Turbulence Kinetic Energy
P_n	Poisson Distribution Probability
Q_i	Droplet Moment
Q_0	Total Drop Number
Q_1	Sum of Drop Radii
Q_2	Sum of Squares of Drop Radii
Q_3	Sum of Cubes of Drop Radii
r	Radius
Re	Reynolds Number
S	Source Term
t	Time
U	Velocity

V	Radial Velocity
V	Volume
$v(d)$	Volume Size Distribution
We	Weber Number
x	Coordinate Direction
X	Weighting Factor

Greek Symbols

α, β	Spray Cone Angles
α_R	Rosin–Rammler Parameter
γ_k	Volume Fraction of kth group
δt	Time Step
ε	Dissipation Rate
θ	Void Fraction
μ	Dynamic Viscosity
ν_1	Liquid Turbulent Viscosity
ρ	Density
σ	Surface Tension
σ	Turbulent Prandtl Number
σ_v	Turbulence Damping Coefficient
Φ_i	Moment Averaged Quantity
Φ	General Dependent Variable

Subscripts

0	Inlet
32	Sauter Mean
b	Bag Breakup
cell	Cell
coal	Coalescence
coll	Collision
eff	Effective
g	Gas
i	Moment Index
in	In
inj	Injection
j	Vector (Free) Index
k	Turbulent Kinetic Energy
l	Liquid
lam	Laminar
m	Mass
out	Out
p, *q*	Mean Diameter Parameters
Q_i	Moment
R	Rosin–Rammler
rel	Relative

s Stripping Breakup
sep Separation
t Inside Radius
U_{ki} Velocity Component

REFERENCES

1. J. C. Beck, *Computational Modelling of Polydisperse Sprays without Segregation into Droplet Size Classes*, Ph.D. thesis (UMIST, 2000).
2. J. C. Beck and A. P. Watkins, On the modelling of polydisperse sprays without segregation into droplet size classes, *Proc. Royal Society A*, to appear.
3. J. C. Beck and A. P. Watkins, The droplet number moments approach to spray modelling: The development of heat and mass transfer sub-models, *Int. J. Heat Fluid Flow*, to appear.
4. J. K. Dukowicz, A particle-fluid numerical model for liquid sprays, *J. Comput. Phys.* **35**, 229 (1980).
5. C. T. Crowe, M. P. Sharma, and D. E. Stock, *The Particle-Source-in-Cell (PSI-CELL) Method for Gas-Droplet Flows, Trans. ASME J. Fluids Engr*. **99**, 325 (1977).
6. A. D. Gosman and E. Ioannides, Aspects of computer simulation of liquid fuelled combustors, Technical Paper 81-0323 (AIAA Press, Washington, DC, 1981).
7. A. A. Mostafa and H. C. Mongia, On the modelling of turbulent evaporating sprays: Eulerian versus Lagrangian approach, *Int. J. Heat Mass Transfer* **30**, 2583 (1987).
8. F. A. Williams, *Combustion Theory* (Addison-Wesley, Reading, MA, 1965).
9. H. C. Gupta and F. V. Bracco, Numerical computations of two-dimensional unsteady sprays for applications to engines, *AIAA J.* **16**, 1053 (1978).
10. J. C. Beck and A. P. Watkins, The simulation of water and other non-fuel sprays using a new spray model, *Atomization Sprays*, **12**(6), (2002).
11. S. Adam and G. H. Schnerr, Instabilities and bifurcations of non-equilibrium two-phase flows, *J. Fluid Mech.* **348**, 1 (1997).
12. W. A. Sowa, Interpreting mean drop diameters using distribution moments, *Atomization Sprays* **2**, 1 (1992).
13. F. H. Harlow and A. A. Amsden, Numerical calculation of multiphase fluid flow, *J. Comput. Phys.* **17**, 19 (1975).
14. B. E. Launder and D. B. Spalding, *Mathematical Models of Turbulence* (Academic Press, San Diego, CA, 1972).
15. A. P. Watkins, Three-dimensional modelling of gas flow and sprays in diesel engines, in *Computer Simulation for Fluid-Flow, Heat and Mass Transfer and Combustion in Reciprocating Engines*, edited by N. C. Markatos (Hemisphere, Washington, DC, 1989), p. 193.
16. W. E. Ranz, Some experiments on orifice sprays, *Can. J. Chem. Eng.* **36**, 175 (1958).
17. P. J. O'Rourke, *Collective Drop Effects on Vaporising Liquid Sprays*, Ph.D. thesis (Princeton Univ., Princeton, 1981).
18. P. K. Senecal, D. P. Schmidt, I. Nouar, C. J. Rutland, R. D. Reitz, and M. L. Corradini, Modeling high-speed viscous liquid sheet atomization, *Int. J. Multiphase Flow* **25**, 1073 (1999).
19. X. F. Wang and A. H. Lefebvre, Influence of ambient air pressure on pressure-swirl atomisation, *Atomisation Spray Technol.* **3**, 209 (1987).
20. G. B. Wallis, *One-Dimensional Two-Phase Flow* (McGraw–Hill, New York, 1969).
21. A. B. Liu and R. D. Reitz, Mechanisms of air assisted atomisation, *Atomization Sprays* **3**, 55 (1993).
22. H. Nicholls, Stream and droplet break-up by shockwaves, in *NASA SP-194*, edited by D. T. Harrje and F. H. Reardon (NASA, Washington, DC, 1972), p. 126.
23. R. D. Reitz and R. Diwakar, *Structure of High Pressure Fuel Sprays*, SAE Paper 870598 (1987).
24. G. M. Faeth, L. P. Hsiang, and P. K. Wu, Structure and break-up properties of sprays, *Int. J. Multiphase Flow* **21**, 99 (1995).

25. H. C. Simmons, The correlation of drop-size distributions in fuel nozzle sprays, *J. Eng. Power* **99**, 309 (1977).
26. L. P. Hsiang and G. M. Faeth, Near-limit drop deformation and secondary break-up, *Int. J. Multiphase Flow* **18**, 635 (1992).
27. Z. Liu and R. D. Reitz, An analysis of the distortion and breakup mechanisms of high speed liquid drops, *Int. J. Multiphase Flow* **23**, 631 (1997).
28. P. J. O'Rourke and F. V. Bracco, Modelling of drop interactions in thick sprays and comparison with experiment, in *Stratified Charge Auto Engines Conf.* (IMechE, London, 1980), p. 101.
29. M. Orme, Experiments on droplet collisions, bounce, coalescence and disruption, *Prog. Energy Combust. Sci.* **23**, 65 (1997).
30. Y. J. Jiang, A. Umemura, and C. K. Law, An experimental investigation on the collision behaviour of hydrocarbon droplets, *J. Fluid Mech.* **234**, 171 (1992).
31. H. K. Versteeg and W. Malalasekera, *An Introduction to Computational Fluid Dynamics* (Longman, New York, 1995).
32. D. B. Spalding, A novel finite-difference formulation for differential equations involving both first and second derivatives, *Int. J. Numer. Meth. Eng.* **4**, 551 (1972).
33. R. I. Issa, Solution of the implicitly discretised fluid flow equations by operator splitting, *J. Comput. Phys.* **61**, 40 (1986).
34. H. Hiroyasu and T. Kadota, *Fuel Droplet Size Distribution in Diesel Combustion Chamber*, SAE Paper 740715 (1974).
35. W. M. Ren and J. F. Nally, Jr., *Computations of Hollow-Cone Sprays from a Pressure Swirl Injector*, SAE Paper 982610 (1998).
36. J. Abraham, *What Is Adequate Resolution in the Numerical Computations of Transient Jets*?, SAE Paper 970051 (1997).
37. A. P. Watkins and H. Khaleghi, An ad-hoc procedure to alleviate false diffusion effects in computer codes using discrete droplet models, in *Proc. Int. Symp. COMODIA 90*, Kyoto, Japan, 1990, p. 237.
38. J. C. Beck and A. P. Watkins, A novel method for simulating polydisperse fuel sprays, *Proc. I. Mech. E. Conf. on Computational and Experimental Methods in Reciprocating Engines*, London (2000), paper C587/019/2000, p. 89.
39. C. Mundo, M. Sommerfeld, and C. Tropea, On the modelling of liquid sprays impinging on surfaces, *Atomization Sprays* **8**, 625 (1998).
40. I. V. Roisman, L. Araneo, M. Marengo, and C. Tropea, Evaluation of drop impingement models: Experimental and numerical analysis of a spray impact, in *15th Annual Conf. on Liquid Atomisation and Spray*, Toulouse, France, 1999, p. 203.